Title

An analysis of soil moisture dynamics using multi-year data from a network of micrometeorological observation sites

Journal

Advances in Water Resources, 30

ISSN

0309-1708

Authors

Miller, Gretchen R.
Baldocchi, Dennis D.
Law, Beverly E.
et al.

Publication Date

2007-05-01

Peer reviewed

An analysis of soil moisture dynamics using multi-year data from a network of micrometeorological observation sites

Gretchen R. Miller [a,*], Dennis D. Baldocchi [b], Beverly E. Law [c], Tilden Meyers [d]

[a] *Department of Civil and Environmental Engineering, 760 Davis Hall, University of California–Berkeley, Berkeley, CA 94720-1710*

[b] *Department of Environmental Science, Policy, and Management, 137 Mulford Hall, University of California–Berkeley, Berkeley, CA 94720-3110*

[c] *College of Forestry, 328 Richardson Hall, Oregon State University, Corvallis, OR 97331*

[d] *Atmospheric Turbulence and Diffusion Division, National Oceanic and Atmospheric Administration, 456 S. Illinois Ave., Oak Ridge, TN 37830*

Abstract

Soil moisture data, obtained from four AmeriFlux sites in the US, were examined using an ecohydrological framework. Sites were selected for the analysis to provide a range of plant functional type, climate, soil particle size distribution, and time series of data spanning a minimum of two growing seasons. Soil moisture trends revealed the importance of measuring water content at several depths throughout the rooting zone; soil moisture at the surface (above 10 cm) was approximately 20 to 30% less than that at 50 to 60 cm. A modified soil moisture dynamics model was used to generate soil moisture probability density functions at each site. Model calibration results demonstrated that the commonly used soil matric potential values for finding the vegetation stress point and field content may not be appropriate, particularly for vegetation adapted to a water-controlled environment. Projections of future soil moisture patterns suggest that two of the four sites will become severely stressed by climate change induced alterations to the precipitation regime.

Key words: Soil-plant-atmosphere models, Soil moisture, AmeriFlux, Ecohydrology, Water stress, Water balance, Vadose zone, Evapotranspiration.

* Corresponding author. *E-mail address:* gmiller@berkeley.edu (G. Miller)

1 Introduction

The complex interactions between soil, vegetation, and the atmosphere play critical roles in the global hydrologic cycle and the functioning of ecosystems. Mounting evidence suggests that these interactions play a larger role in regulating atmospheric conditions than initially assumed. As more sophisticated climate models are being developed, researchers are becoming increasingly aware of the critical role of soil water availability in simulating water fluxes over land surfaces [1]. Models that do not consider the impacts of rainfall pulses and precipitation regime changes on evapotranspiration [2] and total ecosystem respiration [3] will not accurately model the accompanying climatic responses. Spatial and temporal variations in soil moisture can have a lasting impact on climate factors such as precipitation [4], and the inclusion of subgrid scale soil moisture heterogeneity can improve the performance of global climate models [5].

Numerous soil moisture models have been developed in an attempt to quantify and predict fluxes through the Soil-Plant-Atmosphere Continuum (SPAC). Accurate models should, in some manner, account for all components of the terrestrial water balance: precipitation, evaporation, transpiration, runoff, leakage, and storage. Portions of the balance have well-defined models: the Richards equation (and its various analytical solutions) for the flow of water in the vadose zone [6], the Penman-Monteith equation for evaporation [7], and the Poisson arrival process for rainfall [8]. The main difficulty remains in uniting the models of these various components. Several solutions have been tendered, including a notable probabilistic method originally proposed by Rodriguez-Iturbe et al. [9] and improved in a series of papers by Laio et al. [10,11]. Daly and Porporato provide a review of current research into soil moisture dynamics and emphasize its control on meteorological process, soil biogeochemistry, plant conditions and nutrient exchange [12].

Micrometeorological measurement sites record half-hourly exchanges of carbon dioxide, water vapor, and energy between the biosphere and the atmosphere, as well as state variables such as temperature and vapor pressure deficit. In the past, information about soil moisture at these sites was obtained by laboratory analysis of soil samples or from daily to biweekly measurements taken using in-situ soil moisture probes. These methods have drawbacks, namely low temporal resolution and/or high labor requirements. However, sites within the global FLUXNET community and the AmeriFlux network of research sites in the Americas are being encouraged to collect continuous measurements of soil moisture, reportable in half-hour or hourly increments that correspond to energy and trace gas flux measurements. These types of measurements are well-suited for comparison to models that predict soil moisture dynamics at a single point.

FLUXNET provides a unique opportunity to examine ecological trends at a variety of sites, allowing analysis to be performed across functional types and climates. The climate gradient and range of vegetation seen by the flux network is wide. Several recent, multi-site studies have been conducted that use the network to investigate broader topics, such as bud-break timing [13] and soil-respiration [14]. AmeriFlux sites have been collecting soil moisture data for several years, however, no studies have yet examined soil moisture dynamics across a range of sites.

In this study, we present an analysis of soil moisture dynamics at four AmeriFlux sites in the continental United States. We use an ecohydrological model [10] to find a probabilistic description of soil moisture dynamics at each site. We detail several methods for parameter estimation and a technique for calibrating the model to match the measured data. We then incorporate predictions of future precipitation patterns and evapotranspiration into the calibrated model to examine the shifts in the soil water balance that may occur due to global climate change.

2 Description of Sites

Four sites with a range of climate, vegetation, and soil type were selected for analysis. Only sites that listed soil type and collected half-hourly soil moisture data for at least two years were included. While half-hourly soil moisture is listed as a core AmeriFlux measurement, the majority of Ameriflux sites do not measure and/or report soil moisture values at this temporal resolution. Although many sites collect it on a weekly or biweekly basis, shorter measurement intervals are necessary to fully capture the response to precipitation events and the accompanying wetting and drying cycles.

Data for each site was obtained from the AmeriFlux network of ecosystem observation towers [15]. Table 1 lists key characteristics for each site. The following data were included in the analysis: rainfall events and net radiation for each year as gauged at the AmeriFlux station, soil type and grain size distribution as listed in AmeriFlux site information, and half-hourly soil moisture measurements.

The Tonzi and Vaira Ranch sites are located near Ione, CA, in the lower Sierra Nevada Foothills [16]. Tonzi is an oak savanna woodland while Vaira is an annual C3 grassland. The sites are located within 2 km of each other and share a similar Mediterranean climate, with a mean annual temperature of 16.6 ^{o}C and mean annual precipitation of around 560 mm y^{-1} [16]. The Walker Branch watershed site is a mixed deciduous forest located near Oak Ridge, TN. It has a temperate climate with mean annual precipitation of 1333 mm and an average

temperature of 14.4 ^{o}C [17]. The Metolius site is an intermediate age ponderosa pine forest located in the eastern Cascade Mountains near Sisters, OR. It has a temperate climate, with a mean annual precipitation of approximately 360 mm y^{-1} and a mean annual temperature of 7 to 8 ^{o}C [18]. It is the only one of the four sites that receives a substantial amount of snow, which affects soil infiltration patterns during the winter. Precipitation data is collected at all sites using a tipping bucket, which is adapted to measure snowfall at Metolius.

Each site has different seasonal patterns (Table 1). At Walker Branch, the trees are active during the spring and summer, typical of deciduous forests. The Vaira Ranch primarily supports grasses, which are active during the wet, winter months of its mediterranean climate. In addition to these grasses, Tonzi Ranch supports trees, active between March and October. As a result, Tonzi always has actively transpiring vegetation. The Metolius site is in a semi-arid region with typical summer drought. The trees at Metolius are active year-round, however, seasonal differences in temperature, radiation, and vapor pressure deficit significantly reduce transpiration in the winter.

3 Methods

3.1 Data collection

This study used data from each site as reported to and distributed by the AmeriFlux network. Two to four complete years of data were available for each site, generally from 2001 to 2004. Volumetric soil water content is considered a core measurement for AmeriFlux sites, to be taken at a depth between 0 and 30 cm and reported at 30 minute intervals [15]. At the Tonzi, Vaira, and Walker Branch sites, continuous soil moisture measurements were collected using an array of impedance sensors (Theta Probe model ML2-X, Delta-T Devices). These were placed vertically at depths of 5, 20, and 50 cm for Tonzi; 5, 10, and 20 cm for Vaira; and 5, 10, 20, and 60 cm for Walker Branch. Biweekly measurements were also collected at Tonzi and Vaira using segmented, time-domain reflectometer (TDR) probes (MoisturePoint, model 917, Environmental Sensors Equipment Corporation) [16]. At Metolius, continuous measurements were taken at a depth of 0 to 30 cm using a time-domain reflectometer (Campbell CS615). Periodically, measurements were taken throughout the soil profile (10 cm, 30 cm, 50 cm, and 90 cm) using a capacitance probe (Sentek Sensor Technologies).

Each type of probe has a different mode of operation and installation technique. The Campbell TDRs are 30 cm long metal probes, installed either vertically, to obtain an integrated water content or horizontally to record wa-

ter content at a specific depth. Theta Probes have several short sensing rods and measure water content at a point. In general, both derive water content data by measuring the dielectric constant of the porous media. Theta probes determine this from the impedance of the sensing rod array. The Campbell TDRs determine it by propagating waves along the rods, which act as wave guides. Both types are more accurate when calibrated to a specific soil, $\pm$ 0.02 m^3 m^{-3} for both the Theta Probe [19] and the Campbell TDR [20].

Soil samples were periodically collected near the location of the probes. The samples represented a range of wetness values and were obtained at several depths throughout the rooting zone. At Metolius, a calibration curve was developed that related the gravimetric water contents to the voltage response from the TDR probe. At Walker Branch, the manufacturer-provided calibration curve for mineral soil was used, and matched the samples with a random error of around 4%. At Vaira and Tonzi, the half-hourly water content values were compared to the biweekly TDR measurements throughout the site to develop the calibration curve.

3.2 Data analysis

Two main methods of raw data analysis were used: soil moisture histograms and annual time series. The time series charted the course of the daily volumetric water content over several years (Figure 1). From these, trends in year-to-year variability, seasonal patterns, and soil moisture at various depths could be determined. For each site, a series of histograms were generated from the half-hourly degree of soil saturation. The data were grouped in several ways: all years, single years, growing season only, and year-round.

The distinction between volumetric water content and degree of soil saturation is often unclear in the literature, and both terms are used here to describe soil moisture. This treatment is necessary because the model formulates the problem in terms of degree of saturation while the AmeriFlux data is collected as volumetric water content. Volumetric water content is defined as the volume of water in the soil divided by the total volume of the soil (V_w/V_t). Water content and saturation are easily related by the expression $\theta = ns$, where n is soil porosity (unitless), s is degree of saturation in m^3 m^{-3}, and θ is volumetric water content in m^3 m^{-3}. Degree of saturation can also be found by dividing the volume of water by the volume of pore space (V_w/V_p). In this case, the measured values were converted before creating the histograms.

When soil moisture measurements from multiple depths were available, histograms were generated for each depth. However, these did not individually capture the behavior over the entire rooting zone, and a method of finding

depth-averaged soil moisture became necessary. Three methods of finding the average were compared: equal weighting, a zone weighting, and a root weighting.

The arithmetic, or equal weighted, average found the soil moisture as the sum of the measurements at all depths, for instance:

$$\theta_{\text{equal}} = \frac{(\theta_{5\text{cm}} + \theta_{10\text{cm}} + \theta_{20\text{cm}})}{3} \tag{1}$$

The zone weighted depth-average attempted to divide the root zone into portions represented by each measurement. In the following example, the 5 cm probe was assumed to represent the soil between 0 and 7.5 cm; the 10 cm showed the water content between 7.5 and 15 cm; and the 20 cm probe represented the content between 15 and 30 cm.

$$\theta_{\text{zone}} = \frac{(7.5 * \theta_{5\text{cm}} + 7.5 * \theta_{10\text{cm}} + 15 * \theta_{20\text{cm}})}{30} \tag{2}$$

Following Baldocchi et al. [16], the root weighted, depth-averaged soil moisture (m^3/m^3) was determined by:

$$\theta_{\text{root}} = \frac{\int_{Z_r^0} \theta(z)(\mathrm{d}p(z)/\mathrm{d}z)\mathrm{d}z}{\int_{Z_r}^{0} (\mathrm{d}p(z)/\mathrm{d}z)\mathrm{d}z} \tag{3}$$

where z, depth, is positive downward and Z is the depth of the rooting zone. Here, $p(z) = 1 - b^z$, where b is a curve-fitting parameter. The b values used previously for Tonzi and Vaira were 0.94 and 0.976, respectively [16]. Jackson et al. reported b as 0.966 for temperate deciduous forests [21], which was used for Walker Branch.

The depth-averaging process tempered the extreme high and low values that could be found at the surface, but which were not indicative of the overall moisture in the rooting zone. For Vaira, a site with relatively shallow soil, the weighting method did not significantly affect the histogram (Figures 2a and c). However, the histograms at Walker Branch had different shapes depending on weighting technique (Figure 2b and d). There measurements taken simultaneously throughout the rooting zone frequently differ by 0.10 $m^3\ m^{-3}$.

Estimating the average value in the soil profile was more difficult at Metolius, where hourly measurements were limited to the upper 30 cm of the soil profile. Using the periodic Sentek FDR measurements, average soil profiles were generated for the wet, dry, and transitional periods using linear regression. The linear equations were then transformed so that given a half-hourly measurement between 0 and 30 cm, they could be used to estimate the water content

at points throughout the rooting zone. The equations were then integrated using the formula described above, yielding an estimated average water content over the rooting zone.

3.3 Model description

The model used in this research generates a probability density function (pdf) for steady-state soil moisture conditions at a point. It was originally developed by Rodriguez-Iturbe and colleagues in 1999 [9] and has been further described and modified in a series of papers by Laio, Porporato, Ridolfi, and Rodriguez-Iturbe in 2001 [10,11]. The model provides a realistic, quantitative description of the temporal dynamics of the soil moisture, while making the simplifications necessary to find an analytical solution. It has previously been shown to compare well with field data for sites with warm, wet growing seasons and dry, temperate winters. This section will attempt to provide the reader with a brief overview of the model. For more detailed information, the authors recommend the references mentioned above as well as the book *Ecohydrology of Water-Controlled Ecosystems: Soil Moisture and Plant Dynamics* [22].

The foundation of the soil moisture dynamics model is the water balance at a point. This is given by the equation:

$$nZ_{\mathrm{r}}\frac{\mathrm{d}s(t)}{\mathrm{d}t} = R(t) - I(t) - Q[s(t),t] - E[s(t)] - Lk[s(t)] \tag{4}$$

where n is the soil porosity, Z_{r} is the rooting depth, R is the rainfall rate, I is the amount of rainfall lost to canopy interception, Q is the runoff rate, E is the evapotranspiration rate, and Lk is the leakage. The (t) symbol is used to signify that the rate or amount is a function of time, while $s(t)$ indicates that it is a function of the soil moisture at a given time. The first three terms (R, I, Q) represent the amount of infiltration into the rooting zone, while the last two terms (E, Lk) define the amount of water lost from it. The sum of evapotranspiration and leakage forms the loss function, denoted by χ and shown graphically in Figure 3.

In this model, four points are critical to determining the shape of the loss function: s_{h}, s_{w}, s^*, and s_{fc}. These represent the degree of soil saturation at the hygroscopic point, the vegetation wilting point, the vegetation stress point, and the soil field capacity, respectively. The first three correspond to a matric potential (Ψ) in the soil. The hygroscopic point for soils, Ψ_{h} occurs at 10 MPa. The matric potential at the wilting Ψ_{w} and stress points Ψ_{s} are dependent on vegetation type. Wilting generally occurs at around 1.5 MPa for grasses and crops, but can reach up to 5 MPa for trees and plants in semi-arid environ-

ments. Little data is available on the stress point, but the value 0.03 MPa is recommended by the developers of the model. A water retention curve can be used to determine the values of these points in a specific soil, as shown in Figure 4. In this model, s_{fc} is "operationally defined as the value of soil moisture at which the hydraulic conductivity $[K_{\mathrm{s}}]$ ... becomes negligible (10%) compared to the maximum daily evapotranspiration losses, E_{max} ... [22]." Field capacity can also be determined by examining TDR measurements to find the steady-state soil moisture after a wetting event, a somewhat subjective practice, or by using a given pressure, such as -0.01 MPa [6].

In the soil moisture dynamics model, rainfall is treated as a Poisson process, with a rate of arrival equal to λ, and $1/\lambda$ equal to the mean time, in days, between rainfall events. The amount of rainfall occurring during an event (α) is described by an exponential probability density function. Interception capacity (Δ) describes the amount of rainfall that can accumulate on vegetation during a rainfall event; rainfall above this threshold amount reaches the ground. It is included in the model as a modifier to α. Runoff occurs once the soil is completely saturated ($s = 1$).

Because of the stochastic nature of rainfall, the soil water balance can only be described in a probabilistic manner. In this framework, the soils degree of saturation over a given period of time can be modeled as a probability density function (pdf). The derivation of the equation is beyond the scope of this overview, although it can be found in the references cited earlier. In this model, $p(s)$ is the steady state pdf of soil moisture, which can be found using the equations below:

$$p(s) = \begin{cases} \frac{C}{\eta_{\mathrm{w}}}\left(\frac{s-s_{\mathrm{h}}}{s_{\mathrm{w}}-s_{\mathrm{h}}}\right)^{\frac{\lambda'(s_{\mathrm{w}}-s_{\mathrm{h}})}{\eta_{\mathrm{w}}}1} e^{-\gamma s} & \text{if } s_{\mathrm{h}} < s \leq s_{\mathrm{w}} \\ \frac{C}{\eta_{\mathrm{w}}}\left[1+(\frac{\eta}{\eta_{\mathrm{w}}}1)\left(\frac{s-s_{\mathrm{w}}}{s^*-s_{\mathrm{w}}}\right)\right]^{\frac{\lambda'(s^*-s_{\mathrm{w}})}{\eta-\eta_{\mathrm{w}}}-1} e^{-\gamma s} & \text{if } s_{\mathrm{w}} < s \leq s^* \\ \frac{C}{\eta}e^{-\gamma s+\frac{\lambda'(s-s^*)}{\eta}}\left(\frac{\eta}{\eta_{\mathrm{w}}}\right)^{\frac{\lambda'(s-s_w)}{\eta-\eta_{\mathrm{w}}}} & \text{if } s^* < s \leq s_{\mathrm{fc}} \\ \frac{C}{\eta}e^{-(\beta+\gamma)s+\beta s_{\mathrm{fc}}}\left(\frac{\eta e^{\beta s}}{(\eta m)e^{\beta s_{\mathrm{fc}}}+me^{\beta s}}\right)^{\frac{\lambda'}{\beta(\eta-m)}+1}\left(\frac{\eta}{\eta_{\mathrm{w}}}\right)^{\frac{\lambda'(s^*-s_{\mathrm{w}})}{\eta-\eta_{\mathrm{w}}}} e^{\frac{\lambda'(s_{\mathrm{fc}}-s^*)}{\eta}} & \text{if } s_{\mathrm{fc}} < s \leq 1 \end{cases} \tag{5}$$

where

$$\eta_{\mathrm{w}} = \frac{E_{\mathrm{w}}}{nZ_{\mathrm{r}}} \tag{6}$$

$$\eta = \frac{E_{\mathrm{max}}}{nZ_{\mathrm{r}}} \tag{7}$$

$$m = \frac{K_{\mathrm{s}}}{nZ_{\mathrm{r}}(e^{\beta(1-s_{\mathrm{fc}})}1)} \tag{8}$$

$$\beta \sim \frac{\ln\left(\frac{0.1E_{\max}}{K_{\mathrm{s}}}\right)}{\ln\left(s_{\mathrm{fc}}\right)} \tag{9}$$

$$\gamma = \frac{nZ_{\mathrm{r}}}{\alpha} \tag{10}$$

$$\lambda' = \lambda e^{-\frac{\Delta}{\alpha}} \tag{11}$$

In these equations, C is an integration constant. Although it has an analytical solution, the value of C can be found by normalizing $p(s)$ so that:

$$\int_{s_{\mathrm{h}}}^{1} p(s)\mathrm{d}s = 1. \tag{12}$$

3.4 Model application and modifications

Laio et al. [10] cautioned that two conditions need to be fulfilled to apply the steady state results: the climate must be characterized by time invariant parameters throughout the growing season, and the degree of saturation at the start of the growing season should not be very different than the mean steady state condition. The first requirement is met only for the Walker Branch and Vaira sites, which have relatively stable climates during their growing seasons. The year-round growing seasons at Tonzi and Metolius complicate the modeling procedure. The second requirement suggests that soil moisture storage is occurring during wetter periods not in phase with the growing season. However, the soil moisture plots for Tonzi and Vaira suggest that soil water stored during winter periods does not provide a significant amount of moisture during the dry summer periods; the drop in soil moisture is rapid (less than 25 days) and dramatic (around 50%). If significant amounts of storage were occurring, the soil moisture depletion would not be as rapid or as large. At Metolius, the decline is slower, occurring over around 50 days, but no less intense at around 70%. Storage or tapping of deep water sources could be a significant component at this site during days 100 to 175.

Laio et al. [23] also investigated seasonal variations in potential evapotranspiration and its relationship to mean soil moisture. They concluded that delays in the response of the mean soil moisture to rainfall and evapotranspiration forcings could limit the validity of the steady state solution, especially at sites with deep rooting zones and moderate rainfall. With the exception of Walker Branch, the sites experience low to moderate rainfall, but they do not have active soil depths greater than 1.1 meters.

To adapt the model for application at Metolius and Tonzi sites, we developed

a simple weighting method. For example, at Tonzi, the year was divided into two parts based on the wet and dry seasons. The wet season corresponded to the winter when only grass was active, and the early spring when the trees began to bud. The dry season occurred during summer months when only the trees were active. The model was applied to find two different pdfs using a separate set of parameters for each one. A composite pdf was then created by weighting the individual pdfs ($p_{\mathrm{wet}}(s)$, $p_{\mathrm{dry}}(s)$) by the fraction of the year covered by each season (f_{wet}, f_{dry}) as shown below:

$$p(s) = f_{\mathrm{wet}} p_{\mathrm{wet}}(s) + f_{\mathrm{dry}} p_{\mathrm{dry}}(s) \tag{13}$$

We will refer to this as the quasi-steady-state model.

A two-season division was also necessary for Metolius: one season for low potential evaporation during the winter and another for high potential evaporation during the summer. Rainfall parameters, once adjusted for the timing of the snowmelt, were similar for both seasons. To incorporate the effects of snow at the site, the timing of the snowmelt was determined by tracking the soil temperature. Sudden increases in the soil temperature indicated a snowmelt event, which was recorded as a "rainfall" event. This change increased the amount of precipitation per event and the time between events, much as a summer drought would.

3.5 Model parameter estimation

The soil moisture dynamics model uses multiple parameters to estimate a pdf of soil moisture at a given site. Two parameters, average time between rainfall events (λ) and average amount of rainfall per event (α), were calculated directly using the precipitation data reported to AmeriFlux (Table 2). At sites with distinctive wet and dry seasons, separate values were calculated. Interception capacity (Δ) was estimated using data on similar species given by Breuer et al. [24]. The soil parameters (K_{s}, s_{h}, s_{w}, s^*, s_{fc}, n) were estimated using water retention curves, as described in Section 3.3.

The computer program Rosetta [25] was used to generate the water retention curves (WRCs). Rosetta predicts the parameters needed to create the WRC for a soil (including n and K_{s}) using a database of soil particle size distributions. These parameters can then be used in a equation created by Mualem [26] that describes the volumetric water content as a function of soil matric potential ($\theta = f(\Psi)$). Rosetta is an appropriate choice for predicting the function parameters at these sites because it was developed using soils from temperate to subtropical climates in North America and Europe and is heavily biased towards soils with high sand, moderate silt, and low clay contents [25].

Using a function instead of direct measurements to create the WRCs was advantageous in this case, because it allowed for the demonstration of a more general approach, which can be applied to other sites. The problems related to direct measurements of water retention (difficulty, expense, and experimental limitations) can be avoided using these estimates [27]. For the Tonzi, Vaira, and Walker Branch soils, laboratory measurements of the matric potential at various water contents were also collected using the WP4 Dewpoint PotentiaMeter (Decagon Devices) following the manufacturers recommended procedure [28]. The measurements and the WRCs compared favorably for most water content values, however, the laboratory tests were unable to duplicate very low and very high pressures, so these portions of the WRCs could not be confirmed.

Critical soil moisture points for each site were identified using the soil water retention curves. The soil hygroscopic point (s_{h}), also known as the residual saturation, was generated as a parameter from Rosetta and is also visible as the inflection point of the WRC. The remaining critical points are more difficult to identify, primarily because they are plant and climate based. Laio et al. [10] indicate that most vegetation in water-controlled ecosystems begins to experience water stress at a soil matric potential of -0.03 MPa and wilt at -3.0 MPa, although this can be highly variable. This variability is visible at the Tonzi site, where the wilting point of the seasonal grasses was found to be around -2.0 MPa while the nearby trees could continue transpiring below -4.0 MPa [16]. At Metolius, ponderosa pine begin to show water stress at a pre-dawn leaf water potential of -0.5 MPa, and tree transpiration declined to 0.3 mm d^{-1} below -1.6 MPa [29].

In consideration of the uncertainty associated with critical point predictions, a range for each point was generated (Table 3). The range incorporated both the uncertainty in the WRC prediction and in the appropriate soil pressure head. Ranges for the wilting point water content corresponded to a pressure head of -4 MPa to -2 MPa. The stress point range corresponded to pressures of -0.04 MPa to -0.02 MPa. Field capacity ranges were determined by using field measurements after rain events and by finding the water content corresponding to -0.01 MPa and to a hydraulic conductivity of 0.45 mm d^{-1} (around 10% of an assumed E_{max}). Values for the hygroscopic and wilting points showed the smallest ranges, while the stress point and field capacity have much more variability.

The remaining parameters, E_{max} and E_{w}, were more difficult to estimate. Evaporation from soil (E_{w}) depends on a variety of factors, including atmospheric conditions, depth to groundwater water surface, soil cover, and soil texture [6]. Maximum evapotranspiration E_{max} is the daily loss of water through both soil evaporation and plant transpiration, assumed to be constant between s^* and $s = 1$ and decreasing linearly between s^* and s_{w}.

To estimate the atmospheric forcing on transpiration, the half-hourly value of $E_{\max}$ was calculated using the Priestly-Taylor equation [30] as follows:

$$E_{\max} = 1.26 \frac{e'_{\mathrm{s}}}{(e'_{\mathrm{s}} + g)\, L} (R_{\mathrm{n}} - G) \tag{14}$$

where g is the psychometric constant and L is the latent heat of water. The terms G and R_{n} are the half-hourly net radiation and the ground heat flux measured using each sites the flux tower. The saturation vapor pressure derivative with respect to temperature, e'_{s}, is found using the equation:

$$e'_{\mathrm{s}} = \frac{2576.9 exp\left(\frac{17.27 * T_{\mathrm{a}}}{237.3 + T_{\mathrm{a}}}\right)}{(240.97 + T_{\mathrm{a}})^2} \tag{15}$$

where T_{a} is the air temperature in ^oC. To find the daily value for $E_{\max}$, the half-hourly values were summed.

It should also be noted that $E_{\max}$ is synonymous with the terms potential or equilibrium evapotranspiration (E_{eq}), commonly used in the hydrology literature. Unlike other models of evapotranspiration such as the Penman-Monteith equation [31], stomatal conductance is not included in this estimate because it pertains only to the atmospheric drivers.

The equilibrium evapotranspiration predicted by the Priestly-Taylor equation compares well with pan evapotranspiration [32] and evapotranspiration over rangeland [33] and crops [34]. Correlation coefficients ranging from $r^2 = 0.79$ to 0.90 were reported in these studies. However, the equation did not perform as well in studies of deciduous [35] and coniferous [36] forests, where values for the leading term in Equation 14 were found to be between 0.72 and 1.0, lower than the standard 1.26.

The daily actual evapotranspiration (E_{act}), measured at each site using the flux tower, was compared to the equilibrium evapotranspiration. At each site, the data were binned into appropriate time intervals, and the mean E_{eq} and E_{act} were found for each bin (Table 4). By comparing these values, we can determine if the evapotranspiration at a site is limited by the atmospheric demand ($E_{\mathrm{eq}} \leq E_{\mathrm{act}}$) or by the availability of water to the vegetation ($E_{\mathrm{eq}} > E_{\mathrm{act}}$) [16]. Based on this criterion, all sites are water-limited throughout the year, with the exception of Metolius during the winter season. The values found in this study are consistent with the year-round, average evaporation values previously cited in the literature: 1.6 mm d^{-1} for Walker Branch [35], 0.81 mm $\mathrm{d}^{-1}$for Vaira, 1.0 mm d^{-1} for Tonzi [16], and 0.77 mm d^{-1} at Metolius [29].

The accuracy of E_{act} depends on the error associated with the measurements of latent heat flux ($L * E_{\mathrm{act}}$) collected at the micrometeorological towers. Anthoni et al. [37] estimated errors in the latent heat flux to be $\sim \pm$ 15% at a ponderosa pine site in Metolius, OR very similar to the one studied here. At Tonzi and Vaira, an annual bias error of 6%, or 0.06 mm d^{-1}, was estimated for latent heat flux[16]. When the evapotranspiration measurements collected by the tower at Walker Branch were compared to the values obtained using the catchment water balance, the mean annual difference between the two was 60 mm y^{-1}, approximately 10% [38].

3.6 Model testing and calibration

The model generated pdfs were compared with the measured histogram. The histograms were created using the root-weighted, depth-averaging technique (Section 3.2) in order to be representative of the entire root zone. Although the model cannot capture the system's behavior exactly, due to random noise, it should correctly depict the general shape of the histogram, capturing both the location (degree of saturation) and height (normalized frequency) of the peaks. In all cases, the model results were qualitatively different from the measured results in these respects. This difference was attributed to poor initial estimates for one or more parameter values. A method for calibrating the model was needed.

The most uncertain parameters were assumed to be those that were difficult to measure directly and that had either a wide range of possible values (s^*, s_{fc}, Δ) or had to be estimated using methods with unknown accuracy ($E_{\mathrm{max}}, E_{\mathrm{w}}$). Model calibration focused on determining the values of these parameters that best fit the actual data.

Model inversion is typically used to find values for parameters that cannot be easily measured, have a high degree of uncertainty associated with their measurement, or for which measurements are not available. Because the model is computationally inexpensive and the parameter space was relatively small, sophisticated inversion techniques were not necessary. Instead, a direct search approach was used. The range of each parameter was broken into equal increments; a model parameter grid was generated from all possible parameter combinations.

The model was run for each parameter set, and a least squared objective function (J) was used to identify the optimal parameter set:

$$J = \sum_{s=0}^{1} (p_{\mathrm{modeled}}(s) - p_{\mathrm{measured}}(s))^2 \tag{16}$$

where p_{modeled} is the pdf generated by the model and p_{measured} is the normalized histogram.

The best-fitting parameter set is that which generates the smallest value of the objective function ($J_{\min}$). While this method would be inadvisable for a model with a larger parameter space or higher computational requirements, it has the advantage of being easy to conceptually visualize and implement. Using the least squared method makes several assumptions about the data, namely that the measurement errors are normally distributed random variables. In all cases, when the new parameter sets (those associated with $J_{\min}$) were used, the modeled results more closely matched the measured data.

Using inversion, there is a danger of over-fitting the model. By fitting the parameters with limited data sets, there is a chance that the model will only be specific to those years and will not make useful predictions of future behavior. Using multiple years of data that span a large range of conditions minimizes this risk. Only a few years of hourly observations (none with extreme weather) were available for this analysis.

3.7 Forward predictions using the soil moisture dynamics model

Climate change is anticipated to significantly affect precipitation patterns in North America. As a result, vegetation distribution is likely to change in the future, although conflicting scenarios have been presented in the literature. Using two dynamic global vegetation models, Bachelet et al. [39] forecasted the expansion of forests in the Pacific Northwest and the replacement of savannas by forests in north-central California. Based on a regional climate model, Kueppers et al. [40] predicted that the range of California's blue oaks will shrink by up to 59% and shift northward due to 24.5 mm decrease in April through August precipitation. Clearly, the amount and timing of future precipitation will be a significant determinant of vegetation distribution.

To determine how vegetation at the sites studied would respond to changing rainfall and precipitation regimes, the soil moisture dynamics model was used. Detailed temperature and precipitation predictions from a regional climate model were available for the Sierra Nevada foothills region of California, near the location of Tonzi and Vaira Ranches [41]. Using the predicted daily precipitation totals for the years 2000 to 2100, new rainfall parameters (α and λ) were obtained for the two sites by calculating the five year averages for three periods during the time span: early, middle, and late 21st century. The new parameters for the late 21st century indicated decreased rainfall frequency for the spring and summer months, with precipitation event intensity increasing in the spring and falling to nearly half in the summer. Winter parameter

values were relatively constant.

Predicting the values of $E_{\max}$ and E_{w} under altered climatic conditions was more difficult. In Equation 14, $E_{\max}$ is a function of temperature and available energy ($R_{\mathrm{net}} - G$). Assuming that average values of R_{net} and G remain constant and only T_{a} increases, $E_{\max}$ will increase by approximately 3% by mid-century and 7% by late-century at Tonzi and Vaira. However, it cannot necessarily be assumed that the net radiation will remain near its current level. Solar radiation reaching the earths surface may be altered due to changes in cloud cover [42] or atmospheric aerosol concentrations [43]. A sensitivity analysis of Equation 14 shows that a 5% decrease in $R_{\mathrm{net}} - G$ negates the effects of increased temperature on $E_{\max}$. A 5% increase in $R_{\mathrm{net}} - G$ produces an 8% mid-century and a 12% late century increase in $E_{\max}$. Assuming that precipitation and net radiation were related by cloud cover, Kumagai et al. [44] fitted an exponential curve to data from a Bornean tropical rain forest. The curve was then used to predict R_{net} from the predictions of future precipitation patterns at the site. This method was applied to find an appropriate exponential relationship for each site (Tonzi Summer: $R_{\mathrm{net}} = 143.1e^{-0.163P}$, Tonzi Winter: $R_{\mathrm{net}} = 69.5e^{-0.77P}$, Vaira: $R_{\mathrm{net}} = 49.0e^{-0.23P}$, Metolius Winter: $R_{\mathrm{net}} = 35.7e^{-0.13P}$, Metolius Summer: $R_{\mathrm{net}} = 152.4e^{-0.15P}$, Walker Branch: $R_{\mathrm{net}} = 117.4e^{-0.016P}$). Based on these curves, Tonzi and Vaira were predicted to experience a 4% increase in year-round $E_{\max}$ by mid-century, and a 10% late century increase.

Although detailed climate predictions were not available for the other sites, recent global climate models provided generalized predictions for Oregon and Tennessee. By 2090, a 20% increase in summer precipitation [45] and a 1.3 to 6.5 ^oC increase in maximum summer temperature is anticipated in the southeastern U.S. Combined, these result in a 3 to 7% increase in $E_{\max}$.

In the Pacific Northwest, winter precipitation is expected to increase while summer precipitation decreases [46]. Average temperatures are anticipated to increase by 4.1 to 4.6 ^oC in the summer and 4.7 to 5.9 ^oC in the winter. Nolin and Daly [47] showed that warming could change the snowfall accumulation patterns in regions of the Pacific Northwest, including the Metolius area. Precipitation would be more likely to fall as rain, rather than snow, reducing the mean time between precipitation events during the winter, as represented by the parameter $1/\lambda_{winter}$. To model these changes, the precipitation parameters for each site were changed by 10 and 20%, in the appropriate direction. These changes result in an 11 to 20% winter increase in $E_{\max}$, and an 11 to 14% summer increase.

4 Discussion

4.1 Water content time series and histograms

The three sites that had distinctive dry periods in the present climate also demonstrated a distinctive drop in water content at the beginning of the dry season. At the Northern California sites, Tonzi and Vaira, this initially occurred around day 150 and continued until approximately day 300. This pattern indicates that the soil at these sites does not store any appreciable amount of water and reaches a new equilibrium quickly after a change in rainfall regimen. A similar pattern occurred during summer at Metolius, however, the drop in content was less abrupt. The Walker Branch site showed soil moisture that was fairly constant year round, consistent with the more regular rainfall pattern observed.

The water content stress points, as determined by the water retention curves, were compared to the plots of soil moisture (Figure 1). These plots indicated that the trees at Tonzi and Metolius spent a substantial portion of the growing season under water stress. At the Walker Branch site, the findings were slightly more complex, since more information about the soil profile was available. Generally, the soil moisture hovered around the stress point, even though the site received over twice the amount of rainfall of Tonzi and around four times that of Metolius. The forest at Walker Branch is denser, with a leaf area index of 6, as compared to 2 and 3 for the other sites. This could indicate that the trees at each site have adapted to the available soil water. Clearly, Walker Branch can support denser vegetation because of more available moisture. This has caused more growth, but not so much that the trees are overly stressed. It is also important to note that at three of the sites, the soil water content never dropped below the wilting point, except in the surface soil layers. Once soil moisture falls below the wilting point at Vaira, the grass senesces, preventing additional transpiration from occurring. Metolius is clearly water stressed during the summer, however, its leaf area index and the vegetations water use do not exceed the water delivering capacity of its environment, which would be evidenced by a reduction of the soil water beyond the wilting point.

Some evidence points to tapping of deep water sources by the trees at the Tonzi site. During the summer months, soil moisture values can drop below the theoretical wilting point for the trees, however, they continue to transpire, albeit at a highly reduced rate. There are two possible explanations: either the trees can endure higher soil matric potential values than previously considered, or they are using another water source not measured by the soil moisture probes. The first explanation is less likely, because as the soil approaches the hygroscopic point, soil matric potential increases exponentially. A decrease

in a degree of saturation by 0.01 (from 0.16 to 0.15), can cause the matric potential to double (from -5 MPa to -10 MPa). The second explanation is also supported by the work of Lewis and Burgy [48] who showed that several oak species, including blue oaks, could extract groundwater from fractured rocks at depths of up to 24 m.

Water content patterns also revealed the importance of measuring water content throughout the root zone (Figure 5). Many sites collected measurements only in the top portion of the root zone. However, on average, surface water contents were significantly less than those taken deeper in the root zone. At Walker Branch, the surface measurement was 20% less than the measurement at 60 cm. At the more arid sites, the difference was more significant with the 5 cm measurement an average of 23% less than that at 50 cm at Tonzi and 45% less than that at 20 cm measurement at Vaira. At Metolius, a similar comparison using the periodic full root zone data indicated that the measurements collected at 10 cm depth were, on average, 37% less than those collected at 90 cm.

The sites with clear dry seasons (Tonzi, Vaira, and Metolius) have strongly bimodal distributions of half-hourly, depth averaged soil water content (Figure 7). Walker Branch had a unimodal distribution skewed towards the lower water contents. For the sites that recorded soil moisture at several depths (Tonzi, Vaira, and Walker Branch), the year-to-year variations appeared to vary less with increasing depth. Walker Branch and Vaira have limited growing seasons, from days 111–311 and days 304–110 respectively. When non-growing season data was excluded (Figure 7), the Vaira histogram shifted toward higher soil moisture levels, while the Walker Branch peak shifted toward higher soil moisture levels and increased in variance.

Histograms such as these may be useful in plant physiology models that predict the carbon and water fluxes at a site. Including soil moisture as a stochastic variable could lead to more probabilistic predictions of these fluxes, perhaps through the use of Monte Carlo methods. The stochastic soil moisture approach could be a useful compromise between vegetation models which neglect soil moisture constraints on plant processes and fully-coupled models which, at great computational expense, describe flow throughout the soil-plant-atmosphere continuum.

4.2 Hydraulic Redistribution

Hydraulic redistribution occurs when plant roots passively move water through the rooting zone along gradients of high to low matric potential [49]. Generally, water flows upward through the roots from deep, wet layers of soil and is

released into the shallow, dry soil layers; however, downward and lateral flow can also be induced. In field studies, hydraulic redistribution may be confused with other mechanisms of soil water transport, such as capillary rise, which take place without the influence of vegetation.

To test for hydraulic redistribution, the diurnal patterns of water content were examined. The following temperature correction equation was used on the CS615 readings at Metolius: $\theta_{\text{corrected}} = \theta - (T_{\text{s}} - 20) * (-0.000346 + 0.019\theta - 0.045\theta^2)$ [20], where T_{s} is the soil temperature. The Theta probes have not been shown to have a temperature dependency [19], so no correction was applied. During the summer periods when no rain occurs at Tonzi, the soil moisture at 20 cm experiences daily fluctuations in θ of around 0.002, with the peak occurring at 2200 hours and the minimum occurring at 1000 hours (Figure 6a). While this small increase seems unlikely to influence transpiration, it could, when integrated over the length of the rooting zone, provide for 1.2 mm d^{-1} il moisture at the surface has daily fluctuations of around 0.005, with a peak at 1530 hours and a minimum at 0430 hours. A similar pattern occurs at the Metolius site; during the summer, the daily peak occurs around 0630 and the minimum occurs around 1200 hours. The difference was more pronounced, around $\theta = 0.014$. The analysis could not be performed at Walker Branch because water content was reported to two significant figures, not sufficient to detect changes of this magnitude.

These diurnal fluctuations were similar to those observed by Meinzer et al. [49] in a study of several tropical savannas and temperate coniferous forests. They observed that hydraulic redistribution was possible once soil matric potential fell below approximately -0.2 to -0.4 MPa, which is roughly equivalent to $\theta \leq 0.15$ at these sites.

Some evidence against hydraulic redistribution remains. A similar, although smaller, diurnal pattern (Figure 6b) occurred at Vaira even after the grass had senesced, leading to the conclusion that a water transport mechanism other than hydraulic redistribution was acting, possibly upward water vapor flux (capillary rise) during the day followed by condensation at night. Based on this observation, soil moisture and matric potential measurements alone are not sufficient to demonstrate hydraulic redistribution; studies attempting to do so should include other evidence, such as isotopic tracer results or root sap flow measurements.

4.3 Inverse soil texture effect

The inverse soil texture theory states that in dry climates, the most developed vegetation can be found on sandy soils, while in wet climates, it can be found

in finer soils [51]. Based on the principle of water conservation, it asserts that the most suitable soil for a climate is one that loses the least water through evaporation or leakage. In dry climates (less than 500 mm y^{-1}), loss to evaporation from upper soil layers is higher [6]; soils that lose the least to evaporation, such as sands, have an advantage in supporting vegetation. In wetter climates, loss to leakage is the higher than loss to evaporation, and sandy soil becomes a disadvantage. Thus clays, which slow leakage, support denser vegetation in wetter environments. These properties are related to the shapes of the water retention curves for each type of soil.

This effect is prominent when considering the Northern California sites. Although the two have very similar climates, Vaira supports less vegetation than Tonzi. Their soils have the same clay content, but Tonzi has a 13% higher sand content. Metolius, which supports a pine forest, receives even less rainfall, however, its sand content is at 62%, over 30% higher than Vaira, which supports only grass. Walker Branch, which supports an oak forest, has a soil grain distribution very similar to Vaira's, an advantage in wetter climates. This evidence supports assertions made by Fernandez-Illescas et al. [52], which used the soil moisture dynamics model (Section 3.3) to examine species coexistence at a water stressed site in Texas.

4.4 Probability density functions

The final pdfs and their corresponding histograms are shown in Figure 7. The best model fit was found for the Metolius site, with a minimum objective function value ($J_{\min}$) equal to 30. Good fits were also found for Vaira Ranch ($J_{\min} = 89$), Tonzi Ranch ($J_{\min} = 59$), and Walker Branch Watershed ($J_{\min} = 46$). This result may be related to the rooting depth at each site; Metolius had the deepest roots and the best fit while Vaira had the shallowest roots and worst fit. The shallow rooting depth causes greater susceptibility to rainfall pulses and more frequently changing water contents, making the data at Vaira noisier. However, the difference in performance was not great, and the modeled pdfs captured the correct shape and location of the peaks. Even though Metolius and Tonzi are not ideal sites to model, the modifications mentioned in Section 3.3, coupled with careful model calibration, appear successful.

Accurate parameter value estimation was critical to the accuracy of the model. Model calibration procedures increased model accuracy, decreasing the objective function by over 80%, in some cases. The most sensitive parameters were also the most difficult to determine with accuracy, $E_{\max}$ and s^*. Calibration showed that the originally estimated values of $E_{\max}$ did not necessarily produce a good fit between the data and the model. The calibrated $E_{\max}$ values (E_{inv})

were up to 50% different from the estimates (Table 4). Calibration results for interception capacity, Δ, ranged from 0.3 to 2.5 mm, roughly corresponding to ranges given by Breuer et al. [53] for species similar to the ones at these sites.

The stress points found through model calibration (Table 5) did not correspond to the matric potentials suggested by the literature. For Ψ_{s^*}, -0.03 MPa is too negative for trees acclimated to semi-arid conditions and too positive for those acclimated to wet conditions. For grasses at Vaira, the matric potential at the stress point was around -0.25 MPa, much more negative than originally presumed.

At Tonzi, the value of E_{inv} was much less than predicted during the winter. Several possible explanations exist for the difference: the equation used to predict $E_{\max}$ was in error, the root zone was being kept moister by some water source besides precipitation (e.g. hydraulic redistribution), or the trees were tapping water below the lowest measurement location. To explore the question, the uncertain parameters in the model were set to reasonable values ($E_{\max} = 3.5$, $s^* = 0.65$, and $\Delta = 1.4$) while the precipitation values were altered. The pdf matched the histogram when $\alpha \approx 0.05$ 1/d and $\lambda \approx 11$ mm, double the measured value. Additionally, the average evapotranspiration measured during the dry season is 141 mm, more than double the average precipitation, 45 mm. The rooting zone is remaining wetter than anticipated based on the precipitation. Some process that prevents the water in the rooting zone from being depleted through transpiration must be occurring, either tapping of deep water sources, hydraulic redistribution, or capillary rise. As a result, the best-fitting $E_{\max}$ values are low, not reflecting the effects of the additional water.

4.5 Soil moisture under climate change scenarios

The predictive soil moisture pdfs (Figure 8) were evaluated to determine how climate change could potentially increase plant stress. The classification scheme proposed by Porporato et al. [2] divides the water balance at a site into "dry", "intermediate-stressed", "intermediate-unstressed", and "wet" categories based on the shape of its pdf.

The predicted precipitation changes should have little impact at the Walker Branch site, which moves from the "intermediate-unstressed" to the "wet" category. The grasses at the Vaira Ranch site were placed in the "intermediate-unstressed" category for both current and future scenarios. While the site is semi-arid, the grasses die once the soil water content falls below a certain level for a sufficient duration, so their growing season does not include the drier

summer months. The increased precipitation during the winter and spring months may prolong the growing season of the grasses or cause the dominant species to change [54].

The results from Tonzi and Metolius are harder to classify using this system, since they are bimodal. Currently, both sites fall under the "intermediate-stressed" category in the summer. During the winter, Metolius is "intermediate-unstressed" and Tonzi is "wet". In future scenarios, Metolius becomes more seasonally extreme, "dry" in the summer and "wet" in the winter. Tonzi becomes extremely "dry" in the summer and stays "wet" in the winter. The trees at these sites will likely not survive the very dry summers unless they are able to access deeper water resources through root tapping and hydraulic redistribution [40].

Timing of precipitation appears to be the defining factor determining how the soil moisture dynamics at a site will be altered due to climate change. Kumagai et al.[44] addressed the issue of soil moisture dynamics and climate change in a tropical rainforest, concluding that at their site, the pdf of soil moisture was not extremely sensitive to the predicted changes in precipitation. Their results are similar to those for Vaira and Walker Branch, where precipitation during the growing season increased, while year-round precipitation remained the same or decreased. Alternately, Porporato et al. [2] showed dramatic changes in the pdf representing a grassland when the frequency but not the total amount of precipitation was altered. These changes are similar to those at Tonzi and Metolius, where predictions indicate increased annual precipitation, but more time between summer rainfall events.

5 Conclusions

We applied a probabilistic model from the ecohydrological literature [10,22] to describe and predict the behavior of soil moisture dynamics at four different AmeriFlux sites with a range of soil textures, plant types, and climate. Several techniques for analyzing AmeriFlux soil moisture data and incorporating it into the model were presented, including depth-averaging methods and parameter value estimation. Using a simple inversion method for model calibration, the "best-fitting" parameter values for each site were found. Based on the calibrated parameters and estimates of future precipitation and evapotranspiration, the model was used to predict changes in the soil moisture regime due to climate change.

This study suggests that for AmeriFlux sites where soil moisture dynamics are critical to vegetation response, extra care should be taken when collecting soil moisture data. The AmeriFlux network is currently planning to upgrade

soil moisture measurements such that moisture profiles are measured with automated capacitance probes (daily measurements) to as deep as possible to characterize the soil profile throughout the rooting zone of the dominant species. When this is implemented, it will improve our ability to characterize and model soil water transport.

The steady-state probabilistic model of soil moisture dynamics [10]can be used successfully under a variety of site conditions, if appropriate modifications are made. Sites with year-round growing seasons should be divided into several segments corresponding to the dominant species phenology or hydraulic regime, and the results for each weighted to form a year-round pdf. Each time segment should have different evaporation and precipitation parameter values. In cases where different plant types at a site have alternate growing seasons, changes to the soil stress points, rooting depth, and interception capacity may also be appropriate. Parametrization should be done carefully; parameter values should be taken, to the extent possible, from data measured at the site. When parameter values are highly uncertain, a simple inverse modeling technique may be used to determine them with greater confidence. Because seasonality is very important with respect to evaporative potential, the model uses an average taken over a season (winter or summer) when generating soil moisture probability density functions (pdfs). However, assuming a constant evaporative potential may be a significant source of error. The discrepancy between the estimated and calibrated values of $E_{\max}$ may due to this assumption or may be caused by the error inherent in predicting $E_{\max}$ from an empirical equation. It may also be due to vegetation using deeper sources of water than those measured.

Using inversion to calibrate the model had the advantage of obtaining effective, or integrated, parameters over the entire rooting depth. The stress points determined from model inversion were not consistent with previous expectations. The matric potential at the estimated stress point for grasses was less negative than that for trees, indicating that transpiration from grass would begin to decline at higher soil moisture values. The model calibration results for both Tonzi and Vaira Ranches indicate that this might not be an accurate assumption. For grasses, stress began at -0.2 MPa; for trees, it began at -0.009 MPa. One explanation for this behavior could be that trees regulate transpiration more efficiently. A higher stress point indicates that water conservation begins to occur earlier, increasing the range of soil moisture values between the stress point and wilting point. Grasses have a smaller range, and therefore use water less efficiently. An alternate explanation is that a process such as hydraulic redistribution or capillary rise is keeping the rooting zone wetter than the precipitation data would indicate, or that the trees are able to access deep sources of water.

Comparing the results for the trees at Tonzi to the inversion results for Walker

Branch and Metolius, this trend was also apparent. Vegetation at Walker Branch typically experiences the least water stress and has a stress point at -0.064 MPa. Metolius and Tonzi experience more stress and have less negative stress points, indicating much larger ranges between stress and wilting points. Again, trees that begin decreasing transpiration at higher water contents will make more efficient use of available water. On the plot of evaporation as a function of degree of saturation (as in Figure 3), the slope of the line between the wilting point and stress point will be steepest for grasses, will decrease for non-drought tolerant trees, and will be the flattest for trees adapted to water stress. These results support the conclusion that the matric potential at the stress point may be highly variable by plant type and that the suggested value of $\Psi_{s*} = -0.03MPa$ is not appropriate for many sites.

Climate models predict that precipitation patterns at these sites will be altered as the earth warms. While only minor alterations in the soil moisture dynamics were predicted at the Walker Branch and Vaira sites, climate change is predicted to have a much more substantial impact at Tonzi and Metolius. Although average annual precipitation may remain relatively constant or increase, changes in the frequency and timing of this precipitation could increase the stress on the trees at these sites. The question remains: when vegetation at a site experiences near constant, severe stress, will the ecosystem quickly or gradually adapt through changing vegetation type?

The stress points and corresponding soil matric potentials are important, and relatively unknown, factors needed to determine how vegetation responds to a changing climate. Further studies to determine these values based on field observations should be performed to confirm these preliminary findings, and the analysis should be extended to other sites. The impact of spatial heterogeneity of soil and vegetation on the accuracy of such models should also be examined, once soil moisture data becomes available for a wider range of AmeriFlux sites. Additional research into the relationship between increased time spent under water stress and changes in species type may also be appropriate.

Acknowledgements

This material is based upon work supported under a National Science Foundation Graduate Research Fellowship to G. Miller. The authors would like to acknowledge Yoram Rubin at the University of California-Berkeley for his contributions to the paper through discussions of soil moisture and inverse modeling. They would also like to thank Xingyuan Chen for her comments on the paper and Liukang Xu for her laboratory assistance.

References

[1] Feddes R, Hoff H, Bruen M, Dawson T, Rosnay P, Dirmeyer P, Jackson R, Kabat P, Kleidon A, Lilly A, Pitman A. Modeling root water uptake in hydrological and climate models. B Am Meteorol Soc 2001; 82(12): 2797–2809.

[2] Porporato A, Daly E, Rodrguez-Iturbe I. Soil water balance and ecosystem response to climate change. Am Nat 2004; 164(5):625–632.

[3] Xu L, Baldocchi D, Tang J. How soil moisture, rain pulses, and growth alter the response of ecosystem respiration to temperature. Global Biogeochem Cy 2004; 18: 1–10.

[4] Pielke R. Influence of the spatial distribution of vegetation and soils on the prediction of cumulus convective rainfall. Rev Geophys 2001; 39(2): 151-177.

[5] Gedney N, Cox P. The sensitivity of global climate model simulations to the representation of soil moisture heterogeneity. J Hydrometeorol 2003; 4(6): 1265–1275.

[6] Hillel D. Environmental soil physics. San Diego: Academic Press; 1998.

[7] McNaughton K, Jarvis P. Using the Penman-Monteith equation predictively. Agr Water Manage 1984; 8: 263–278.

[8] Onof C, Chandler R, Kakou A, Northrop P, Wheater H, Isham V. Rainfall modelling using Poisson-cluster processes: a review of developments. Stoch Env Res Risk A 2000; 14: 384–411.

[9] Rodriguez-Iturbe I, Porporato A, Ridolfi L, Isham V, Cox DR. Probabilistic modeling of water balance at a point: the role of climate, soil and vegetation. Proc R Soc Lond A 1999; 455: 3789-3805.

[10] Laio F, Porporato A, Ridolfi L, Rodrguez-Iturbe I. Plants in water-controlled ecosystems: active role in hydrologic processes and response to water stress II. Probabilistic soil moisture dynamics. Adv Water Res 2001; 24: 707–723.

[11] Laio F, Porporato A, Fernandez-Illescas C, Rodrguez-Iturbe I. Plants in water-controlled ecosystems: active role in hydrologic processes and response to water stress IV. Discussion of real cases. Adv Water Res 2001; 24: 707–723.

[12] Daly E, Porporato A. A review of soil moisture dynamics: from rainfall infiltration to ecosystem response. Environ Eng Sci 2005; 22(1): 9–24.

[13] Baldocchi D, Black T, Curtis P, Falge E, Fuentes J, Granier A, Gu L, Knohl A, Pilegard K, Schmind H, Valentini R, Wilson K, Wofsy S, Xu L, Yamamoto S. Predicting the onset of net carbon uptake by deciduous forests with soil temperature and climate data: a synthesis of FLUXNET data. Int J Biometeorol 2005; 49: 377–387.

[14] Hibbard K, Law B, Reichstein M, Sulzman J. An analysis of soil respiration across northern hemisphere temperate ecosystems. Biogeochemistry 2005; 73: 29–70.

[15] Ameriflux website. http://public.ornl.gov/ameriflux/. Oak Ridge National Laboratory. September 2005.

[16] Baldocchi D, Xu L, Kiang N. How plant functional-type, weather, seasonal drought, and soil physical properties alter water and energy fluxes of an oak-grass savanna and an annual grassland. Agr Forest Meteorol 2004; 123: 13–39.

[17] Wilson K, Hanson P, Mulholland P, Baldocchi D, Wullschleger S. A comparison of methods for determining forest evapotranspiration and its components: sap-flow, soil water budget, eddy covariance and catchment water balance. Agr Forest Meteorol 2001; 106: 153–68.

[18] Swartz P, Law B, Wiliams M, Irvine J, Kurpius M, Moore D. Climatic versus biotic constraints on carbon and water flues in seasonally drought-affected ponderosa pine ecosystems. Global Biogeochem Cy 2004; 18: GB4007.

[19] Delta-T Devices. ThetaProbe Soil Moisture Sensor User Manual. 1999.

[20] Campbell Scientific. Instruction Manual: CS615 Water Content Reflectometer. 1996.

[21] Jackson R, Canadell J, Ehleringer J, Mooney H, Sala O, Schulze E. A global analysis of root distributions for terrestrial biomes. Oecologia 1996; 108: 389-411.

[22] Rodriquez-Iturbe I, Porporato A. Ecohydrology of water controlled ecosystems: soil moisture and plant dynamics. Cambridge: University Press; 2004.

[23] Laio F, Porporato A, Ridolfi L, Rodriquez-Iturbe I. On the seasonal dynamics of mean soil moisture. J Geophys Res 2002; 107(15): 4272–4281.

[24] Breuer L, Eckhardt K, Frede HG. Plant parameter values for models in temperate climates. Ecological Modelling 2003; 169: 237–293

[25] Schaap M, Leij F, van Genuchten M. ROSETTA: a computer program for estimating soil hydraulic parameters with hierarchical pedotransfer functions. Journal of Hydrology 2001; 251: 163–176.

[26] Mualem, Y. A new model from predicting the hydraulic conductivity of unsaturated porous media. Water Resour Res 1976; 12: 513–522.

[27] Schaap M, Nemes A, van Genuchten M. Comparison of models for indirect estimation of water retention and available water in surface soils. Vadose Zone J 2004; 3:1455–1463.

[28] Decagon Devices. Generating a soil moisture characteristic using the WP4. 2005.

[29] Irvine J, Law B, Kurpius M, Anthoni P, Moore D, Schwarz P. Age-related changes in ecosystem structure and function and effects on water and carbon exchange in ponderosa pine. Tree Physiol 2004; 24: 753–763.

[30] Priestly C, Taylor R. On the assessment of surface heat flux and evaporation using large-scale parameters. Mon Weather Rev 1972; 100:8192.

[31] Monteith J. Evaporation and environment. The State and Movement of Water in Living Organisms: Symposia of the Society for Experimental Biology 1965; 19: 205-234.

[32] Xu C, Singh V. Evaluation and generalization of radiation-based methods for calculating evaporation. Hydrol Process 2000; 14: 339–349.

[33] Stannard D. Comparison of Penman-Monteith, Shuttleworth-Wallace, and Modified Priestly-Taylor evapotranspiration models for wildland vegetation in semiarid rangeland. Water Resour Res 1993; 29(5): 1379–1392.

[34] Davies J, Allen C. Equilibrium, potential, and actual evapotranspiration from cropped surfaces in Southern Ontario. J Appl Meteor 1973; 12: 649–657.

[35] Wilson K, Baldocchi D. Seasonal and interannual variability of energy fluxes over a broadleaves temperate deciduous forest in North America. Agr Forest Meteorol 2000; 100: 1–18.

[36] Shuttlework W, Calder I. Has the Priestly-Taylor equation any relevance to forest evapotranspiration? J Appl Meteor 1979; 18: 639–646.

[37] Anthoni P, Law B, Unsworth M. Carbon and water vapor exchange of an open-canopied ponderosa pine ecosystem. Agric Forest Meteorol 1999; 95: 151–168.

[38] Wilson K, Hanson P, Mulholland P, Baldocchi D, Wullschleger S. A comparison of methods for determining forest evapotranspiration and its components: sap-flow, soil water budget, eddy covariance and catchment water balance. Agr Forest Meteorol 2001; 106: 153–168.

[39] Bachelet D, Neilson R, Hickler T, Drapek R, Lenihan J, Sykes M, Smith B, Sitch S, Thonicke K. Simulating past and future dynamics of natural ecosystems in the United States. Global Biogeochem Cy 2003; 17(2): 1045–1066.

[40] Kueppers L, Snyder M, Sloan L, Zavaleta E, Fulfrost B. Modeled regional climate change and California endemic oak ranges. P Natl Acad Sci USA 2005; 102(45): 16281–16286.

[41] Maurer EP, Duffy PB. Uncertainty in projections of streamflow changes due to climate change in California. Geophys Res Lett 2005; 32: L03704 doi:10.1029/2004GL021462.

[42] Arking A. The radiative effects of clouds and their impact on climate. Bull Am Meteorol Soc 1991; 71(6):795–813.

[43] Mitchell J, Johns T. On modification of global warming by sulfate aerosols. J Climate 1997; 10: 245267.

[44] Kumagai T, Katul G, Saitoh T, Sato Y, Manfroi O, Morooka T, Ichie T, Kuraji K, Suzuki M, Porporato A. Water cycling in a Bornean tropical rain forest under current and projected precipitation scenarios. Water Resour Res 2004; 40: W01104, doi: 10.1029/2003WR002226.

[45] Burkett V, Ritschard R, McNulty S, O'Brien J, Abt R, Jones J, Hatch U, Murray B, Jagtap S, Cruise J. Potential consequences of climate variability and change for the Southeastern United States. Climate Change Impacts on the United States: A report of the national assessment synthesis team. Cambridge: Cambridge University Press; 2001.

[46] Parson E, Mote P, Mantua N, Snover A, Keeton W, Miles E, Canning D, Ideker K. Potential consequences of climate variability and change for the Pacific Northwest. Climate Change Impacts on the United States: A report of the national assessment synthesis team. Cambridge: Cambridge University Press; 2001.

[47] Nolin A, Daly, C. Mapping "at-risk snow in the Pacific Northwest, U.S.A. J Hydrometeor 2006; In print.

[48] Lewis DC, Burgy, RH. The relationship between oak tree roots and groundwater in fractured rock as determined by tritium tracing. J Geophys Res 1964; 69(12) 2579–2588.

[49] Meinzer F, Brooks J, Bucci S, Goldstein G, Scholz F, Warren J. Converging patterns of uptake and hydraulic redistribution of soil water in contrasting woody vegetation types. Tree Physiol 2004; 24: 919–928.

[50] Pepin S, Livingston N, Hook W. Temperature-dependent measurement errors in time domain reflectometery determinations of soil water. Soil Sci Soc Am J 1995; 59: 38–43.

[51] Noy-Meir I. Desert ecosystems: environment and producers. A Rev Ecol Syst 1973; 4:25–51.

[52] Fernandez-Illescas C, Porporato A, Laio F, Rodriquez-Iturbe I. The ecohydrological role of soil texture in a water-limited ecosystem. Water Resour Res 2001; 37(12): 2863–2872.

[53] Breuer L, Eckhardt K, Frede HG. Plant parameter values for models in temperate climates. Ecol Model 2003; 169: 237–293.

[54] Knapp A, Fay P, Blair J, Collins S, Smith M, Carlisle J, Harper C, Danner B, Lett M, McCarron J. Rainfall variability, carbon cycling, and plant species diversity in a mesic grassland. Science 2002; 298: 2202–2204.

Nomenclature

α	Mean amount of precipitation per rainfall event [mm]
b	Root density model parameter [unitless]
β	Parameter describing drainage in soil moisture model [unitless]
C	Integration constant [unitless]
Δ	Interception capacity of vegetation [mm]
E_{act}	Actual measured evapotranspiration [mm d^{-1}]
E_{eq}	Equilibrium evapotranspiration [mm d^{-1}]
E_{inv}	Value found for E_{max} based on model calibration [mm d$^-$1]
E_{max}	Estimated maximum rate of evapotranspiration [mm d^{-1}]
E_{w}	Estimated rate of evaporation from soil [mm d^{-1}]
e'_{s}	Saturation vapor pressure derivative [kPa $^o\text{C}^{-1}$]
η	Root zone normalized evapotranspiration [d$^-$1]
η_{w}	Root zone normalized evaporation from soil [d^{-1}]
f_{season}	Fraction of a year comprised by a particular season [unitless]
G	Ground heat flux [W m^{-2}]
g	Psychometric constant [kPa K^{-1}]
γ	Root zone normalized average precipitation per event [unitless]
I	Interception rate [mm d^{-1}]
J	Objective function value [unitless]
J_{min}	Minimum value of objective function found during inversion [unitless]
K_{s}	Saturated hydraulic conductivity of soil [mm d$^-$1]
L	Latent heat of vaporization [J g^{-1}]
Lk	Leakage [mm d$^-$1]
$1/\lambda$	Average time between precipitation events [d^{-1}]
$1/\lambda'$	Average time between precipitation events exceeding interception capacity [d^{-1}]
m	Root zone normalized loss from leakage [d^{-1}]
n	Soil porosity [m^3 m^{-3}]
$p(s)$	Probability density function for soil moisture [unitless]
Ψ	Soil matric potential [MPa]

Ψ_{h} Matric potential at the soil hygroscopic point [MPa]

Ψ_{w} Matric potential at the vegetation wilting point [MPa]

Ψ_{s} Matric potential at the vegetation stress point [MPa]

Q Runoff rate [mm d^{-1}]

R Rainfall rate [mm d^{-1}]

r^2 Correlation coefficient [unitless]

R_{n} Net radiation [W m^{-2}]

s Degree of soil saturation [unitless]

s_{h} Degree of soil saturation at hygroscopic point [m^3 m^{-3}]

s_{w} Degree of soil saturation at wilting point [m^3 m^{-3}]

s_{fc} Degree of soil saturation at the field capacity [m^3 m^{-3}]

s^* Soil saturation at stress point [m^3 m^{-3}]

T_{a} Air temperature [^{o}C]

T_{s} Soil temperature [^{o}C]

θ Soil volumetric water content [m^3 m^{-3}]

V_{p} Volume of pore spaces in a soil [m^3]

V_{t} Total volume of soil [m^3]

V_{w} Volume of water contained in a soil [m^3]

z Depth [mm]

Z_{r} Depth of rooting zone [mm]

Table 1
Site Characteristics

Site	Tonzi	Vaira	Metolius	Walker Branch
Location	Ione, CA	Ione, CA	Metolius, OR	Oak Ridge, TN
Vegetation Type	Oak savanna	Grazed C3 grassland	Coniferous forest	Mixed deciduous forest
Climate	Mediterranean	Mediterranean	Temperate	Temperate
Soil Type	Auburn extremely rocky silt loam	Exchequer very rocky silt loam	Sandy loam	Silty loam
Precipitation (mm)	560	560	360	1333
Growing Season	Late October to Mid May for grasses and March to October for trees	Late October to Mid May	Year round	Mid March to Early November
Typical LAI(m^2/m^2)	2	< 2	3	6
Average Annual NDVI	0.52	0.59	0.65	0.64
NDVI Range	0.35-0.79	0.46-0.81	0.23-0.84	0.35-0.88
Years	2002 to 2004	2001 to 2003	2002 to 2004	2003 to 2004

Table 2
Precipitation Parameters

Site		Precipitation (mm)	α_1 (mm)	α_2 (mm)	λ_1 (d^{-1})	λ_2 (d^{-1})
Tonzi	Average	556	9.17	6.59	0.29	0.04
	2002	496	9.15	9.46	0.27	0.022
	2003	616	9.06	3.87	0.35	0.039
	2004	518	9.28	6.42	0.25	0.061
Vaira	Average	441	7.16	–	0.29	–
	2001	389	6.97	–	0.29	–
	2002	494	8.74	–	0.25	–
	2003	439	5.77	–	0.34	–
Metolius	Average	311	8.33	4.72	0.13	0.17
	2002	351	8.24	7.83	0.11	0.13
	2003	306	10.59	3.98	0.12	0.16
	2004	278	6.17	2.36	0.17	0.22
Walker Branch	Average	1258	7.73	–	0.38	–
	2003	922	6.92	–	0.37	–
	2004	1594	8.53	–	0.38	–

Table 3
Soil Characteristics and Critical Soil Moisture Points

Site	Sand	Silt	Clay	K_s	n	s_h	s_w	s^*	s_{fc}
Tonzi	43	43	43	200	0.39	0.147–0.156	0.159–0.200	0.488–0.758	0.59–0.97
Vaira	30	57	13	278	0.42	0.142–0.148	0.157–0.179	0.585–0.836	0.53–0.93
Metolius	62	28	10	387	0.45	0.142–0.146	0.160–0.182	0.456–0.575	0.59–0.99
Walker Branch	28	60	12	322	0.42	0.136–0.145	0.151–0.170	0.589–0.842	0.51–0.93

Table 4
Mean Equilibrium and Actual Evapotranspiration

Site	Season	$\bar{E}_{\text{eq}}$ (mm/d)	$\bar{E}_{\text{act}}$ (mm/d)	E_{inv} (mm/d)
Tonzi	Wet Season	1.22	0.76	1.8
	Dry Season	3.59	0.79	1.9
Vaira	Growing	1.26	0.97	1.0
	Non-growing	2.25	0.44	-
Metolius	Summer	4.35	1.69	3.2
	Winter	0.82	0.76	1.20
Walker Branch	Growing	4.88	2.41	2.4
	Non-growing	1.75	0.55	-

Table 5
Degree of Saturation at Stress Point

Site	s^*	Matric Potential (MPa)
Vaira	0.3	-0.3
Tonzi Grass and Trees	0.3	-0.2
Walker Branch	0.56	-0.06
Metolius	0.68	-0.009
Tonzi - Trees Only	0.85	-0.009

List of Figures

jections from global climate models and represent a 10% and 20% change in precipitation model parameters and the corresponding change in evapotranspiration.

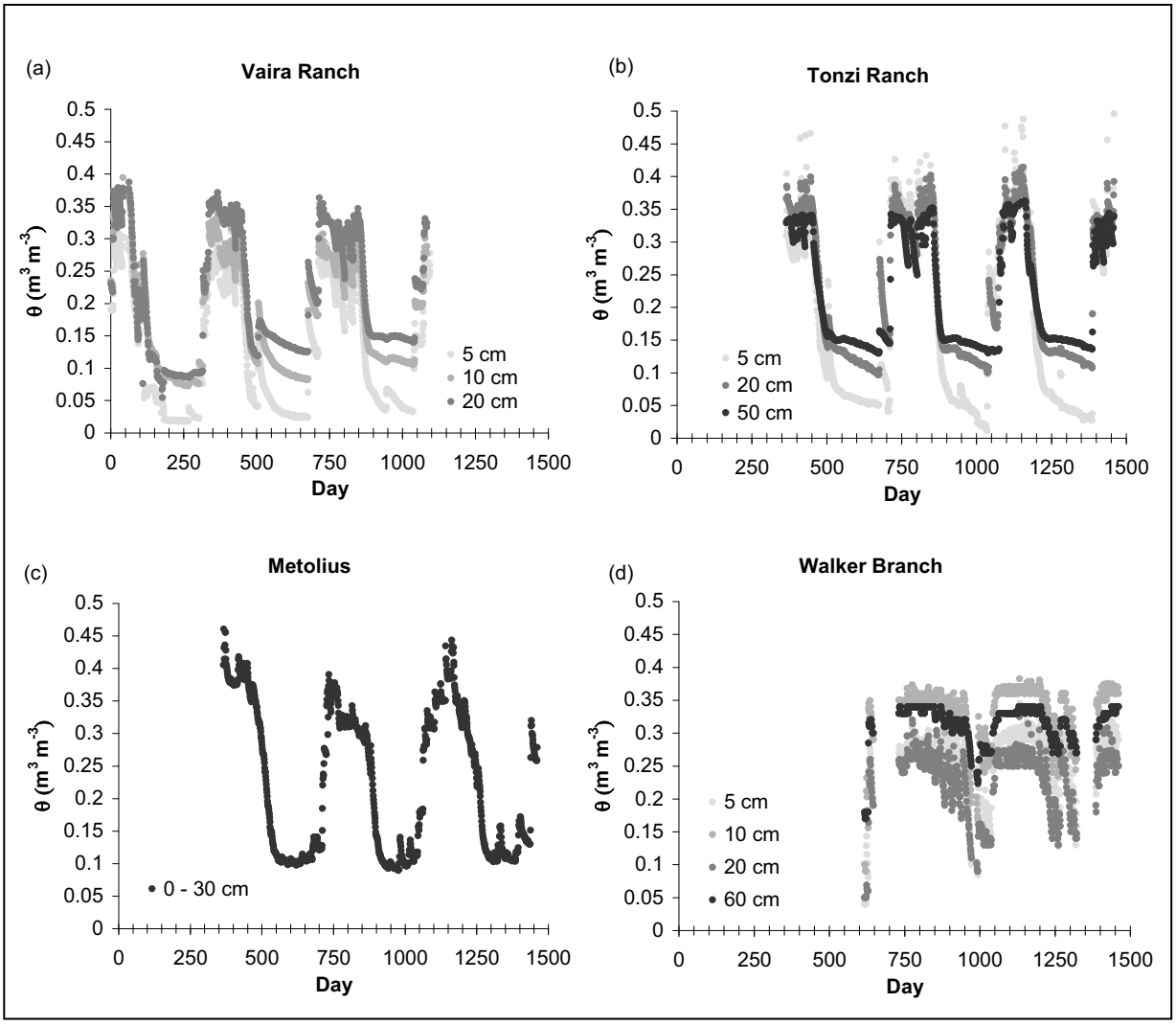

Figure 1: Time series plots of average daily volumetric water content at each site. Vaira (a), Tonzi (b), and Metolius (c) show distinct seasonal patterns in soil moisture, with dry summers and wet winters. Soil moisture at Walker Branch (d) remains fairly steady throughout the year, due to the site's summer precipitation pattern.

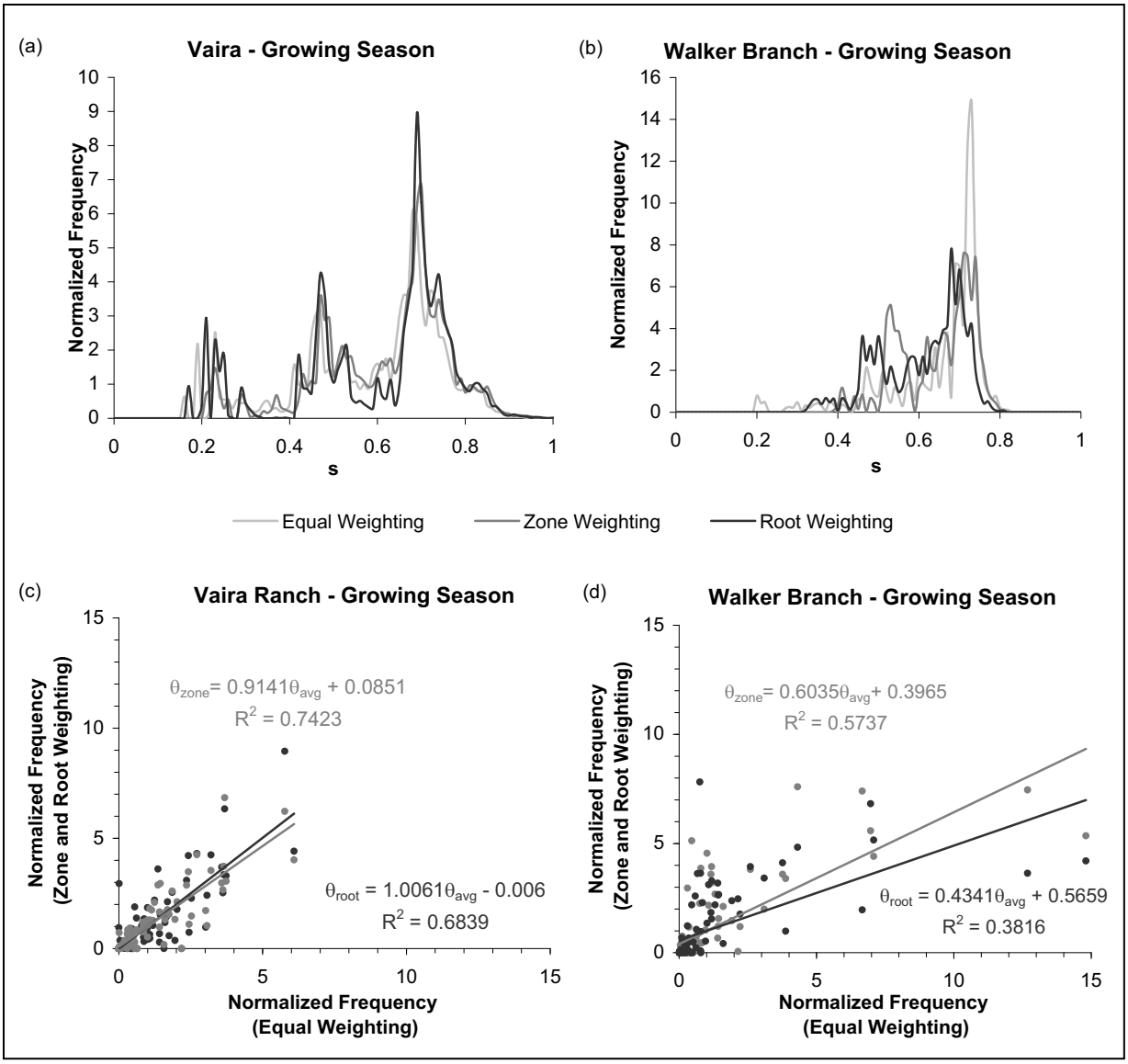

Figure 2: A comparison of soil moisture depth-averaging methods. At Vaira Ranch, the weighting method does not make a qualitative (a) or quantitative (c) difference in the soil moisture histogram. However, at Walker Branch, the three methods deviate considerably, as shown in the plot of the histograms (b) and in the plot of comparing equal weighting to zone and root weighting (d).

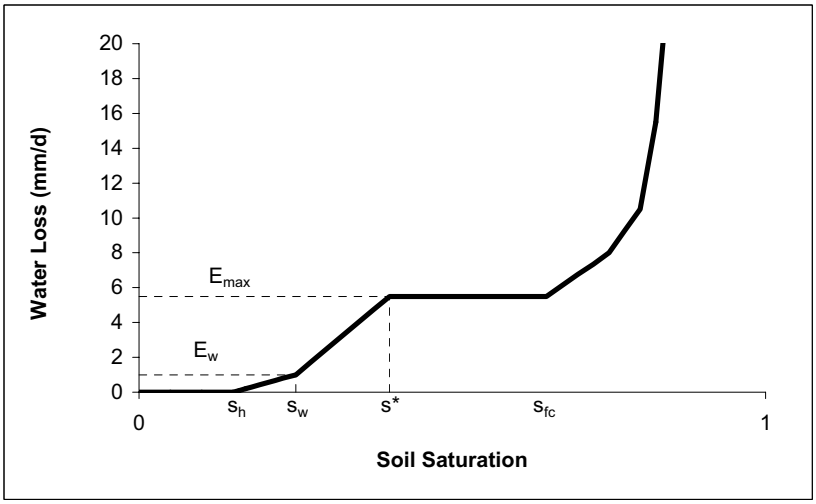

Figure 3: Example soil water loss function for water-stressed environments. Below the wilting point, all loss is determined by evaporation from soil. Between the wilting point and the plant stress point, additional loss occurs due to plant transpiration. Above the field content, soil is losing water at a rate defined by its hydraulic conductivity. (After Laio et al. 2001.)

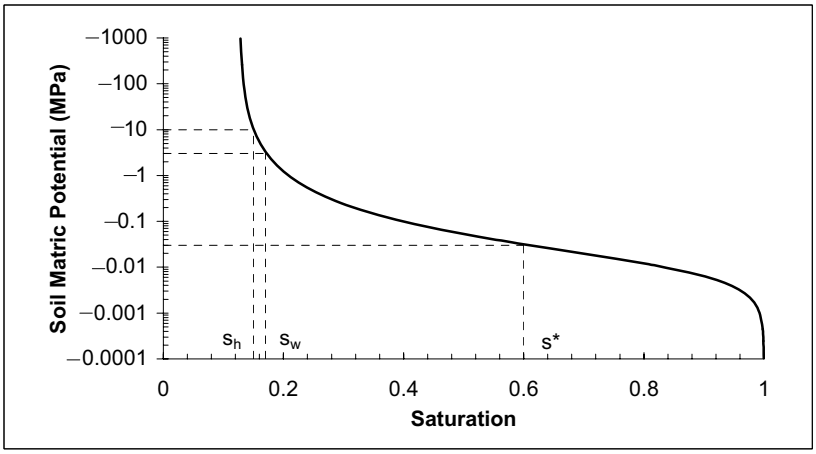

Figure 4: Water retention curve for silt loam used to estimate the soil parameters for the model. The matric potentials anticipated at the hygroscopic, wilting, and stress points are known, and from the curve, the associated degree of saturation is found.

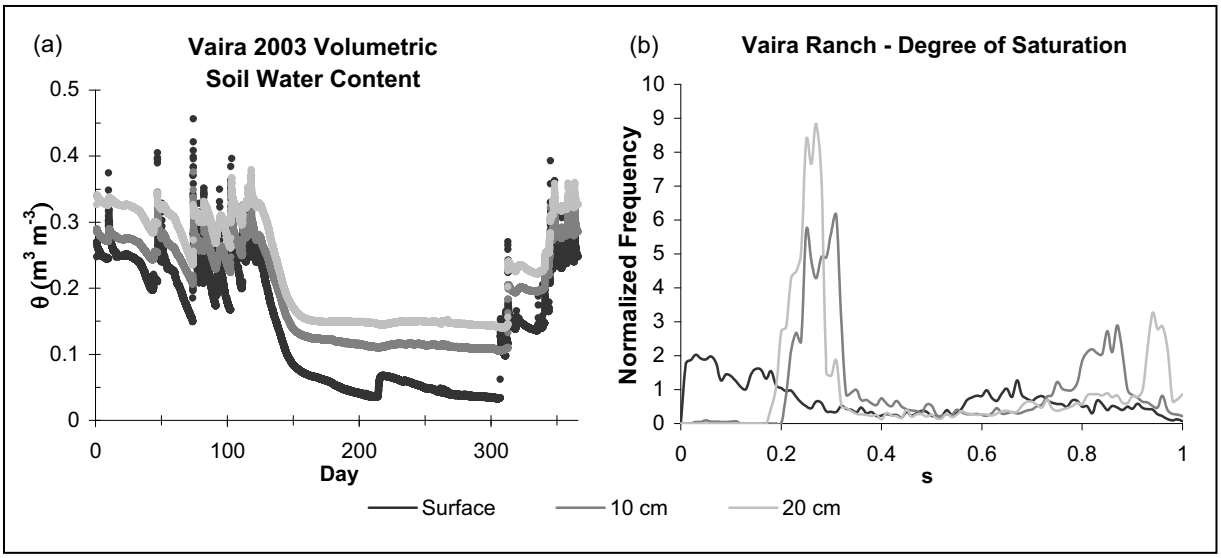

Figure 5: Example of soil moisture time series and histograms at varying depths at same sight. During the summer months, the difference in volumetric water content can be up to 0.1 m^3/m^3 (a), resulting in substantially different histograms for each depth (b).

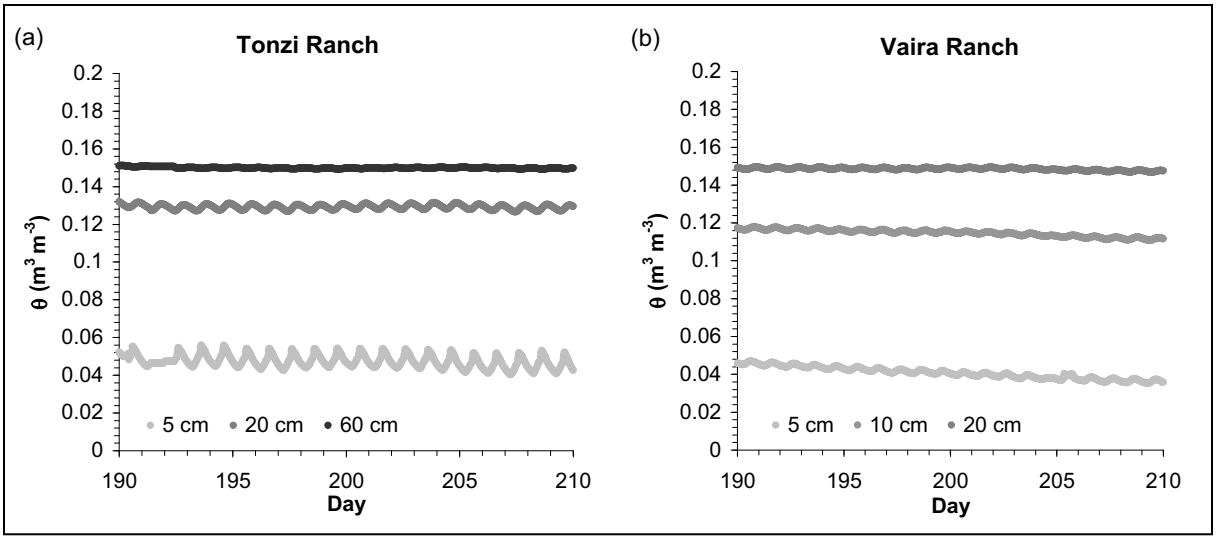

Figure 6: Diurnal fluctuations in soil moisture at the Tonzi Ranch (a) and Vaira Ranch (b) sites. The volumetric water content increases slightly during the nighttime hours.

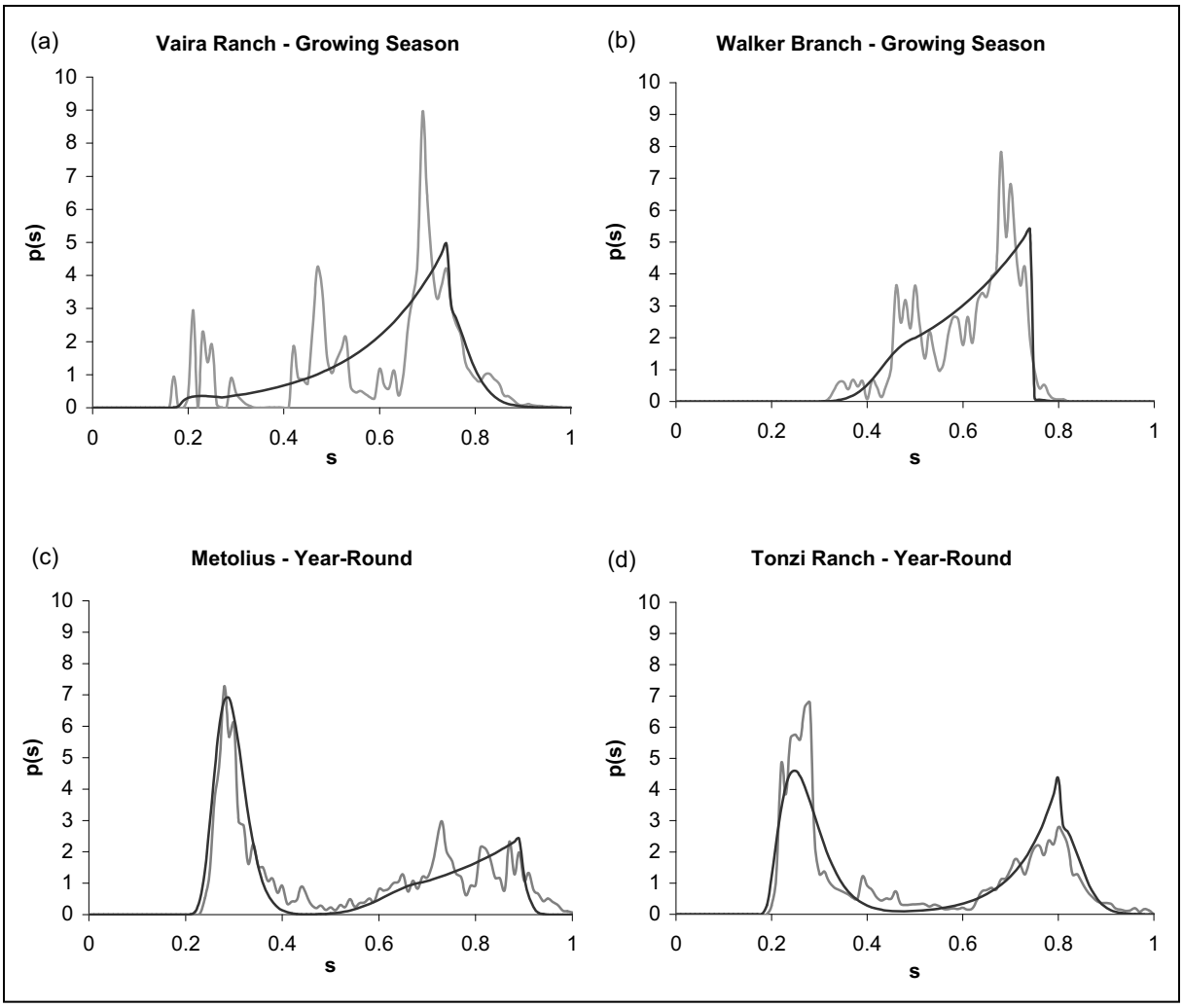

Figure 7: A comparison of measured, depth-averaged data displayed as histograms (gray) and calibrated model results as pdfs (black). The measured and modeled results show good agreement in overall shape, but the model cannot capture all of the variation.

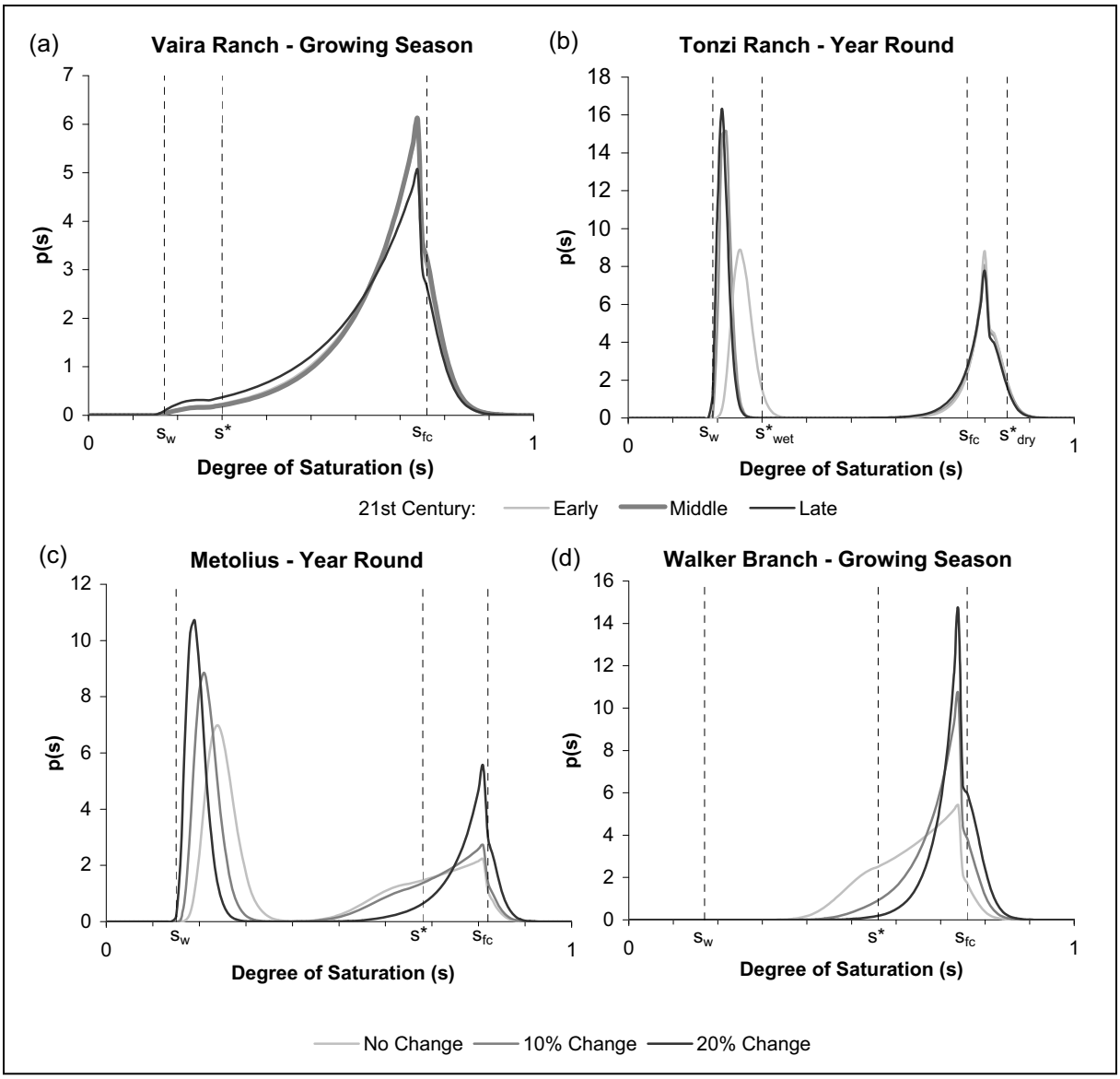

Figure 8: Comparison of pdfs predicting results of alterations in precipitation patterns and evapotranspiration levels due to climate change. The results for Vaira (a) and Tonzi (b) are based on data from a regional climate model. The results from Metolius (c) and Walker Branch (d) are based on regional projections from global climate models and represent a 10% and 20% change in precipitation model parameters and the corresponding change in evapotranspiration.